

ISO-SWS spectra of the carbon stars TX Psc, V460 Cyg, and TT Cyg^{*}

U.G. Jørgensen¹, J. Hron², and R. Loidl²

¹ Niels Bohr Institute, Astronomical Observatory, Juliane Maries Vej 30, 2100 Copenhagen, Denmark

² Institut für Astronomie der Universität Wien, Türkenschanzstrasse 17, 1180 Wien, Austria

Received 10 May 1999 / Accepted 25 January 2000

Abstract. During our open and discretionary time ISO programs we have observed a number of carbon-rich and oxygen-rich AGB stars. We present here a hydrostatic analysis of 3 carbon rich stars, TX Psc, V460 Cyg, and TT Cyg, which show only modest variability.

We identify absorption features of the molecules C₂, CN, CH, CO, CS, HCN, C₂H₂, and C₃ in the three stars. The relative intensities of the corresponding bands put strict limits on the possible values of T_{eff} , $\log g$, and C/O. In particular the ratio of the intensity of the 3 μm band (due to HCN and C₂H₂) and the 5 μm band (due to CO and C₃) is a sensitive measure of the C/O ratio.

We show that our model atmospheres and corresponding synthetic spectra are able to reproduce the observed spectra quite accurately from the visual region through the infrared out to approximately 10 μm . Beyond 10 μm the flux in the observed spectra increases compared to the computed spectra, and the photospheric 14 μm band dominated by C₂H₂ and HCN is almost absent in the observed spectra whereas it is very strong in the synthetic ones. This discrepancy is not an artefact in the reduction or in the SWS response function, but a physical phenomenon in the stars, which does not appear in oxygen-rich giants.

We exclude a so-called “warm molecular envelope” as an explanation of the discrepancies, and suggest that the flux excess at long wavelengths can be interpreted as clumps of ≈ 500 K dense material which obscures about 10% of the photosphere. Weak spectral features seen around 13.7 μm can be understood as even cooler gas, rich in C₂H₂, above the clumps. Other possible models to explain the long wavelength discrepancy between the computed and observed spectra need to be explored too.

Key words: stars: AGB and post-AGB – stars: atmospheres – stars: carbon – molecular processes – stars: variables: general – infrared: stars

Send offprint requests to: uffegi@nbi.dk

^{*} Based on observations with ISO, an ESA project with instruments funded by ESA member states (especially the PI countries: France, Germany, the Netherlands and the United Kingdom) and with the participation of ISAS and NASA

1. Introduction

During our open and discretionary time ISO programs, we have observed a number of carbon- and oxygen-rich AGB stars. Some of the strongly variable stars in our sample were monitored at several phases, some of the less varying stars only once. In a preceding paper (Hron et al. 1998), we analysed the spectra of the strongly variable carbon star R Scl, by use of hydrostatic as well as newly developed hydrodynamic model atmospheres (Höfner & Dorfi 1997; Höfner et al. 1998). In that paper we discussed the possibilities the new hydrodynamic modelling opens up for the analysis of AGB stars, but we also commented on the problems in separating the uncertainties in the input data and relevant physics from the complexity in the treatment of dynamical phenomena (shocks, pulsation, dust formation etc). In the present paper we have chosen to present results from spectra of 3 stars which are much less variable than R Scl and therefore should be described reasonably well by hydrostatic models alone. This enables us to enter into a deeper discussion about methods of the spectral analysis, including the accuracy in the reduction methods, the quality of available input data and the statistical spectral sampling methods.

2. Observations and data reduction

The observations were part of the solicited discretionary time program ZZAGB2PN of Kerschbaum et al. and obtained with the SWS (de Graauw et al. 1996). The spectra were taken with AOT01, i.e. they are full grating scans (2.4 μm to 45 μm). The speeds were either 1 or 2 which results in a typical resolution of 400 (Leech 1998). The pipeline processed data (OLP versions 7.01) were further reduced with ISAP. For all spectra a significant offset between the two scan directions was found in band 2C (7 μm to 12 μm) which was corrected by rejecting the scan direction with the higher flux.

The individual detectors and bands were combined by additive constants if the flux was below 100 to 200 Jy and by multiplicative corrections otherwise. Since some of the spectral features extend across more than one SWS-band and since we wanted to compare also the overall spectral shape, care had to be taken to minimise errors introduced by the band combination. For this reason we used band 2A (4.08 μm to 5.30 μm) as a flux reference. This band is well calibrated and has a wavelength

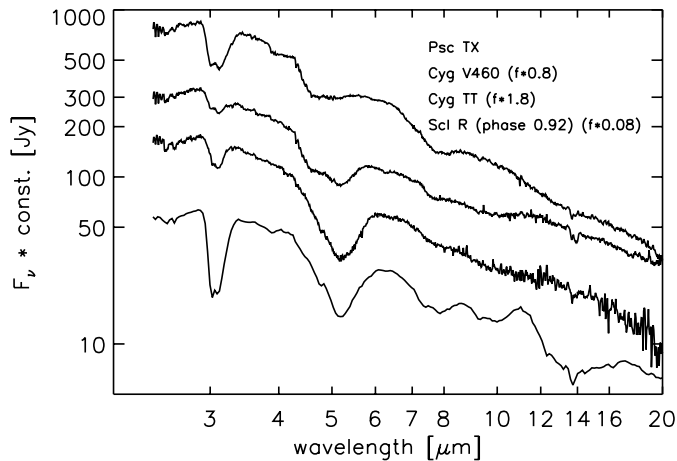


Fig. 1. ISO-SWS spectra of the three stars discussed in this paper (TX Psc, V460 Cyg and TT Cyg starting from the top) and the SRb variable R Scl (bottom). The spectrum of R Scl was obtained at visual phase 0.92 and already discussed in Hron et al. (1998). Note that for V460 Cyg, TT Cyg and R Scl the fluxes have been scaled for a better separation of the stars. The scaling factors are given in brackets.

range such that errors in its absolute flux are not propagated over too many bands. We also extracted the spectra of several calibration stars of earlier spectral type from the ISO archive. This allowed us to optimise the wavelength regions used for joining the bands and to check for systematic effects at the band limits. One such calibration object, the K5 III star HR6705 is shown in Fig. 2 together with a synthetic spectrum computed from a model atmosphere in the same way as we use it for analysing our target stars. We also show the effect of a 5% error in the flux of band 2A (propagated to the other bands in the same way as expected from the data reduction).

From the final spectra we computed flux densities in the L' and the IRAS 12 μm and 25 μm filters. A comparison with ground based photometry (compiled from the literature) and the IRAS point source catalogue showed differences between $\pm 10\%$ and $\pm 20\%$, the differences at 25 μm generally being the largest. This is in agreement with the expectations from the flux variability of our targets, the calibration uncertainty of the SWS and the propagation of a flux error in our reference band to longer wavelengths. For TX Psc all three fluxes are below the literature values and this lower luminosity supports the lower temperature derived from our data compared to previous work (see Sect. 4.4). For V460 Cyg, our flux at 25 μm is 80% larger than the IRAS value while the other fluxes agree within 10%. Since the flux of this star is significantly lower than 100 Jy at these wavelengths, a 10% error in band 2A can easily produce such a large percentage error at long wavelengths. Therefore the overall shape of the spectra of our fainter stars V460 Cyg and TT Cyg is considerably uncertain beyond 20 μm .

The final spectra are shown in Fig. 1 together with a spectrum of R Scl taken near maximum light which was already discussed in Hron et al. (1998). One can note the prominent features of HCN/C₂H₂ at 3 μm and CO/C₃ between 4.3 and

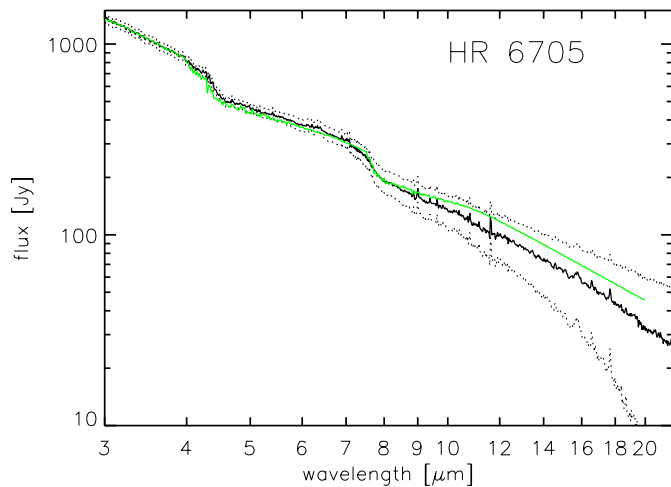


Fig. 2. SWS01 spectrum of HR 6705 (observed at 1998-02-03 with speed 2; thick full drawn line) extracted from the ISO archive compared with a model spectrum (thin full drawn line) for a K5 giant ($T_{\text{eff}} = 3850\text{ K}$, $\log g = 0.0$, $Z = Z_{\odot}$). The dotted lines demonstrate the effect of a 5% error in the flux of band 2A. The major spectral features are the CO fundamental band around 5 μm , the SiO fundamental at 8 μm and the SiO first overtone around 4 μm .

6 μm . Weaker features at 2.5 μm and 3.8 μm are due to C₂ and CS/HCN, respectively.

3. Model atmospheres and synthetic spectrum computation

As mentioned in the introduction, we have chosen the stars presented in this paper such that we expect being able to analyse the spectra with hydrostatic models. The model atmospheres are computed by use of an updated version of the original MARCS code (Gustafsson et al. 1975). Some of the improvements in the present version have been described by Jørgensen et al. (1992), Helling et al. (1996), and Jørgensen (1997). We treat the energy balance in the opacity sampling scheme, and have adopted approximately 10,000 frequency points for the radiative transfer computation. The models are fully self-consistent, and thermodynamic quantities are computed in LTE in approximately 50 depth layers from $\tau_{\text{Ross}} \approx 10^{-6}$ to $\tau_{\text{Ross}} \approx 100$. We include the molecules CO (from Goorvitch & Chackerian 1994), CN (from Jørgensen & Larsson 1990), C₂ (from Querci et al. 1974), CH (from Jørgensen et al. 1996), CS (from Chandra et al. 1995), HCN, C₂H₂, and C₃ (as described in Jørgensen 1997) in the opacity, together with continuum sources as described in Gustafsson et al. (1975).

Although the present version of the MARCS code has the capability of computing the model structure in spherical geometry, we decided to perform the present analysis in plane-parallel geometry. This allows us a more direct comparison with other relevant computations in the literature, which all have been performed in plane-parallel geometry, and therefore to better allow for a discussion of variation in the stellar fundamental parameters between several observations, the impact of different physical input data etc, which is an aim of the present paper. Effects of

sphericity on carbon stars was analysed in detail by Jørgensen et al. (1992). For the stars in the parameter space discussed in the present paper, the effect of sphericity was found to be modest, and the test computations we performed in spherical geometry in the present work did not alter the conclusions derived from plane-parallel models below. This situation is in strong contrast to the cool M-giants, where the effects of sphericity on the structure and the synthetic spectra are known to be much larger (see for example Aringer et al. 1999).

The synthetic spectra are computed with a spectrum program based on the same radiative transfer routines as in the MARCS code, but using a larger frequency set of our opacity samplings, with a resolution of approximately 20,000. With a typical micro turbulence of 3 km/s in cool giants, this resolution corresponds to approximately 5 Doppler half widths per spectrum radiative transfer computation, which provides a much better approximation to the real spectrum than the OS resolution of only approximately 1,000 which was used in our analysis of the spectrum of R Scl (Hron et al. 1998).

Due to the statistical character of the opacity sampling technique, it is necessary to average the OS spectrum over a number of frequencies before it can be compared to an observed spectrum. The presented SWS1 spectra have a resolution of approximately 400, and the corresponding synthetic OS spectra have therefore been averaged over 50 opacity sampling spectral frequencies in order to obtain the same resolution. This results in an OS spectrum which resembles well a “true” synthetic spectrum, i.e. one computed with “infinite” resolution in the radiative transfer solution. When the line density is large there is a tendency for the OS spectrum technique to overestimate the absorption a bit, and vice versa when the line density is small. The higher the frequency density in the sampling the more accurate is the final spectrum.

The OS absorption coefficients used for the model constructions and the synthetic spectrum computations have been improved compared to the versions described in our previous papers. Scaling to laboratory data for HCN, C_2H_2 , and C_3 was introduced where possible. The original data of HCN and C_3 are computed *ab initio* by use of the CASSCF method (see the original papers by Jørgensen et al. 1985 and 1989). Some of the stronger bands which appear in the low resolution stellar spectra are measured in the laboratory with higher accuracy than are achieved *ab initio*. The opacities have therefore been improved by scaling these bands to the laboratory values. For C_2H_2 which is not computed *ab initio*, the scaling is even more important. The method for scaling the bands is based on the theory described in Jørgensen (1990) and Sørensen & Jørgensen (1992). This method makes it possible to keep the correct calculated high-temperature form of the bands (i.e., to include the contribution from many hot bands and adopt the right individual anharmonic frequencies of the contributing hot bands), while still taking advantage of the ground-state intensities measured in the laboratory at room temperature.

The absorption coefficient of C_2 long-ward of $1.1\mu m$ has been scaled in order to match the more recent computation of the Ballik Ramsay band at $2.5\mu m$ due to Goorvitch (1990).

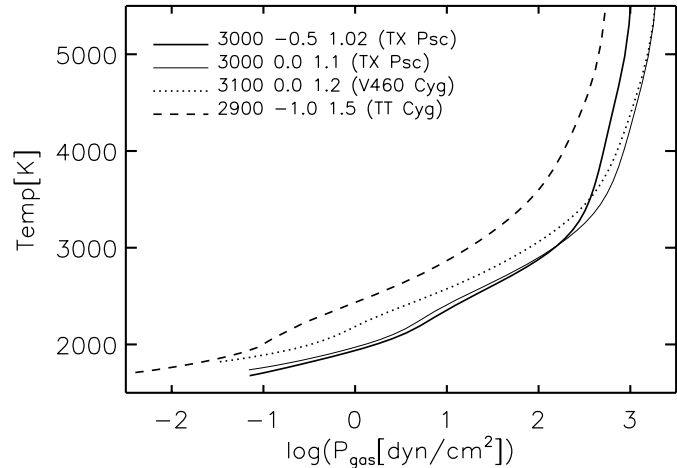


Fig. 3. The temperature versus gas pressure structures of model atmospheres representative for the discussion of the synthetic spectra. The thin and the thick solid line represent two different models for TX Psc which both fit the observed spectrum. Remark the strong similarity in the outer atmosphere (for $T \lesssim 3000$ K) of these two models. Dashed and dotted lines are representative models for TT Cyg and V460 Cyg, respectively. Values of T_{eff} , $\log g$, and C/O are given in the legend.

The computation by Goorvitch (1990) covers only this single band, where it differs substantially (by approximately a factor 10 for the integrated absorption coefficient) from the result of Querci et al. (1974), which has hitherto been used in our model atmosphere computations. Goorvitch (1990) found his results for the $2.5\mu m$ band to be in good agreement with ground based spectra of this band in WZ Cas. Whereas the results by Querci et al. (1974) and the corresponding results by Kurucz (1994) are in reasonably good agreement short-ward of $1.1\mu m$, all three sources of C_2 data disagree substantially with one another in the long-wavelength region.

The introduced scalings for the 4 molecules (C_2 , HCN, C_2H_2 , and C_3) have substantial implications for details in the spectra, but affect the model structure only little because of the limited frequency ranges the changes apply to. Compared to our previous published synthetic spectra and analysis of molecular features (e.g., Hron et al. 1998; Loidl et al. 1999), we note that in our new computations (1) the contribution of C_2H_2 is weaker around $2.5\mu m$ and $3.8\mu m$ and stronger around $7\mu m$ (on the short-wavelength wing of the $8\mu m$ CS band), (2) the contribution of HCN is weaker around $2.5\mu m$, and stronger around $3.8\mu m$ and $8\mu m$, and (3) the contribution of C_2 is weaker in the $2.5\mu m$ region.

4. The spectrum of TX Psc

We observed TX Psc once during our ISO program, where we obtained a SWS1 spectrum from $2.4\mu m$ to $45\mu m$. A higher resolution ISO SWS6 spectrum of TX Psc in the region $2.8\mu m$ to $8.0\mu m$ was published by Aoki et al. (1998), and a lower resolution Kuiper Airborne Observatory (KAO) observation of pieces of the spectrum from $1.25\mu m$ to $5.5\mu m$ was discussed by Goebel & Johnson (1984). The slopes of the three spectra are quite sim-

Table 1. Observations and stellar parameters.

Parameter	TX Psc	V460 Cyg	TT Cyg	Note
Observing Date	2450794.3	2450782.3	2450773.3	
ISO-AOT	SWS01-2	SWS01-1	SWS01-2	
Variability	Lb	SRb	SRb	
Period [d]		180	118	
L/L_{\odot}	5200	17300	2800	(1)
log g ('observed')				
'direct'	-0.7 to +0.0	-1.3 to -0.3		(2)
from T , L and M	-0.6 to +0.1	-1.4 to -0.2	-0.6 to +0.4	(3)
T_{eff}, log g, C/O:				
Walker et al. (1979)	3110			lunar occultations
Ridgway et al. (1980)	3100			lunar occultations
Tsuji (1981)	3070	2850		IR flux method
Lambert et al. (1986)	3030 0.0 1.027	2850 1.06		literature and FTS data
Jørgensen (1989)	3100 -0.5 1.023			fit to KAO IR spectrum
Quirrenbach et al. (1994)	2805			lunar occultations
Dyck & Van Belle (1996)	2900	3200		interferometry
Aoki et al. (1998)	3080 0.0 1.10			IR flux method and ISO-SWS
This work	3100 -0.5 1.023			our fit to literature spectra
This work	3100 0.0 1.1			ditto, but $K_p(C_3) = {}^2K_p(C_3)$
This work	3000 -0.5 1.023	3000 -0.5 1.2	3000 0.0 1.5	$K_p(C_3) = {}^2K_p(C_3)$
This work	3000 -0.5 1.023	3100 -0.5 1.023	3000 0.0 1.2	$K_p(C_3) = {}^1K_p(C_3)$
This work	3000 0.0 1.1	2900 -1.5 1.1	2900 -1.0 1.5	$K_p(C_3) = {}^2K_p(C_3)$
This work			2900 -1.0 1.3	$K_p(C_3) = {}^1K_p(C_3)$

(1) based on HIPPARCOS parallaxes and bolometric magnitudes derived from VJHKL(M) and IRAS photometry.

(2) from distance, angular diameter and mass; ranges are extreme values from $\pm 1\sigma$ of trigonometric parallax and a mass between 1 and $2 M_{\odot}$.

(3) ranges are extremes as in (2), T_{eff} taken from this work for $\log g = -0.5$.

ilar, as are most of the spectral features, whereas the intensity of the $3\mu\text{m}$ band varies substantially between the 3 observations. The $3\mu\text{m}$ band is relatively weak in the KAO spectrum and in the ISO spectrum presented by Aoki et al. (1998), whereas the band is quite strong in our ISO spectrum.

4.1. Our simulations of TX Psc spectra from the literature

Aoki et al. (1998) identified band systems due to HCN, CH, CS, and CO in their spectrum, and found that among the sets of fundamental parameters they tested for their models and synthetic spectra, the set (T_{eff} , log g , C/O) = (3080, 0.0, 1.1) reproduced the observed spectrum best. Lambert et al. (1986) analysed TX Psc based on high resolution FTS spectra and synthetic spectra computed with the MARCS code, and found C/O = 1.027 when log g = 0.0 and T_{eff} = 3030 K were adopted. In the work of Lambert et al. (1986) the computed $3\mu\text{m}$ feature was substantially stronger than the observed one. Jørgensen (1989) reproduced the KAO infrared spectrum, including the $3\mu\text{m}$ feature, with the parameter choice (T_{eff} , log g , C/O) = (3100, -0.5, 1.023) using also MARCS atmospheric models and synthetic spectra.

All the above mentioned values of T_{eff} and log g adopted for the model atmosphere analyses are within the range of estimates given in the literature (see Table 1), and their differences could in principle reflect intrinsic variations in the star. All the analyses

assumed solar composition except for carbon. The C/O value can of course not vary, and the discrepancies in the derived values of the C/O ratio of TX Psc have therefore given rise to some debate in the literature (see e.g. Ohnaka & Tsuji 1996; De Laverny & Gustafsson 1997) which has not been settled yet. All these studies are based on plane parallel, hydrostatic model atmospheres. For the present study, we have computed a small grid of 25 plane parallel, hydrostatic models of TX Psc with T_{eff} adopting the values 2900 K, 3000 K, and 3100 K, and log g values of 0.0, -0.5, and -1.0. We have varied C/O between 1.02 and 1.1, and also varied some of the uncertain physical input parameters within acceptable limits.

We can reproduce well both the SWS6 spectrum of Aoki et al. (1998) and the KAO spectrum with the parameter choice (T_{eff} , log g , C/O) = (3100, 0.0, 1.1) (i.e., approximately the parameter set adopted by Aoki et al. 1998) as well as with the parameters (T_{eff} , log g , C/O) = (3100, -0.5, 1.023) (i.e., the parameter set adopted by Jørgensen 1989). The fit is, however, strongly dependent on the value of the so-called $K_p(C_3)$ which will be discussed in detail below. The reason that both fundamental parameter sets reproduce the spectra basically equally well is the following: An increase of log g from -0.5 to 0.0 enhances the formation of polyatomic molecules relative to diatomic molecules. Therefore intuitively it should increase the intensity of the $3\mu\text{m}$ feature (which in this C/O range is due mainly to HCN). On the other hand, the corresponding increase

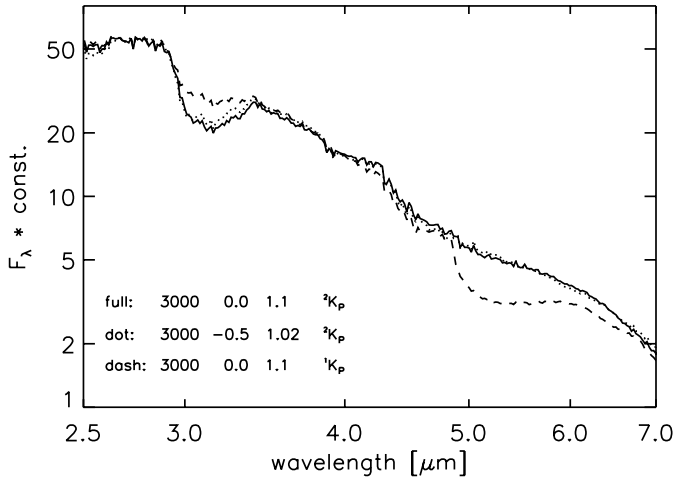


Fig. 4. The resulting synthetic spectra based on models with fundamental input parameters as given in the legend. In spectrum 1 and 2 (labelled 2K_p ; full and dotted lines), $K_p(C_3)$ is based on a recent fit to the JANAF table data, whereas spectrum 3 (labelled 1K_p ; dashed line) is based on $K_p(C_3)$ from the widely used work of Tsuji (1973), as described in the text.

of C/O from 1.023 to 1.1 in the models shifts the balance between C_3 and HCN such that relatively more C_3 and less HCN is formed. The outcome of the simultaneous change of $\log g$ and C/O with the given values is that they almost exactly compensate each other.

In contrast, our models with $(T_{\text{eff}}, \log g, C/O) = (3100, 0.0, 1.023)$ or $(3100, -0.5, 1.1)$ do not reproduce the SWS6 and the KAO spectra.

4.2. The uncertainty in $K_p(C_3)$

One of the important input parameters in the construction of models and synthetic spectra of stars with fundamental parameters close to those of TX Psc, is the so called $K_p(C_3)$ value, which is unfortunately only known with quite a large uncertainty. It expresses the equilibrium between atomic carbon, C_2 and C_3 . $K_p(C_3)$ is actually a function of temperature T , usually expressed as a polynomial in $\Theta = 5040/T$. We tested two different polynomials for $K_p(C_3)$ one is due to a widely used computation by Tsuji (1973 and private communication 1998; hereafter ${}^1K_p(C_3)$), and one is a recent polynomial fit to the JANAF table data due to Ch. Helling (private communication 1998; hereafter ${}^2K_p(C_3)$). Unfortunately, both values are rather uncertain compared to K_p for other molecules, and the JANAF table data do not rely purely on experimental values in the case of C_3 .

With the adoption of the polynomial fit to the JANAF tables (${}^2K_p(C_3)$) we can reproduce the SWS6 and the KAO spectra well with both of the fundamental parameter choices mentioned above, because C_3 plays only a minor role for a spectrum with these parameter choices. But the adoption of the ${}^1K_p(C_3)$ value requires the parameter choice $(T_{\text{eff}}, \log g, C/O) = (3100, -0.5, 1.023)$ as seen in Fig. 4. The reason that this

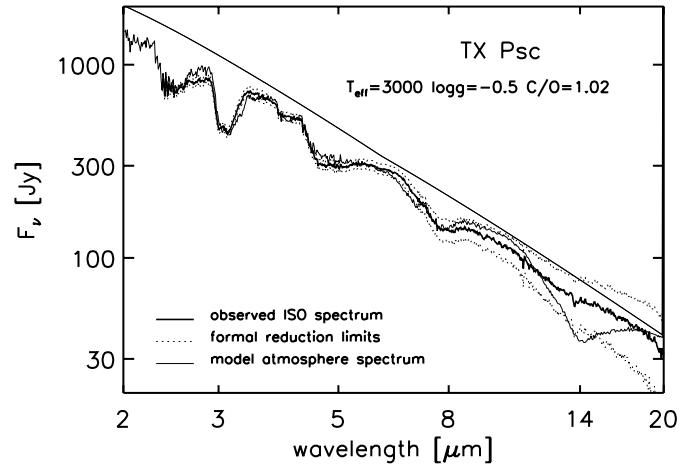


Fig. 5. Our observed SWS1 ISO spectrum of TX Psc together with our synthetic spectrum based on a model with $T_{\text{eff}} = 3000$ K, $\log g = -0.5$, and $C/O = 1.023$. The thick solid line is the observed spectrum. The upper and lower dotted lines are the corresponding observed spectra representing a propagated 5% error in flux band 2A as described in detail in Sect. 2. Upper almost straight thin line is the model continuum, while the thin line spectrum is the synthetic model atmosphere spectrum.

problem did not appear in the analysis of Aoki et al. (1998) (who found a good fit for $(T_{\text{eff}}, \log g, C/O) = (3100, 0.0, 1.1)$ and $K_p(C_3) = {}^1K_p(C_3)$) and in the analyses of Lambert et al. (1986) and of Goebel & Johnson (1984), is that these authors did not include C_3 as an opacity source. The value of $K_p(C_3)$ therefore didn't influence their spectra other than through its indirect effect on the formation of other molecules which were included in their opacity (e.g., HCN, C_2 , C_2H_2 , etc).

The above comparisons show that the SWS6 spectrum and the KAO spectrum can be fitted well with a model of 3100 K and $\log g$ between -0.5 and 0.0 and C/O between 1.023 and 1.1 with the restrictions mentioned.

4.3. Synthetic spectrum simulation of our own ISO observation of TX Psc

Our own SWS1 ISO spectrum shows a much stronger $3\mu\text{m}$ band than the two spectra of TX Psc from the literature. It can not be fitted with any of the parameter choices mentioned above. In fact a reasonable fit cannot be obtained with any model we have tested with $T_{\text{eff}} = 3100$ K. In all such models the computed $3\mu\text{m}$ band is too weak compared to the observed SWS1 $3\mu\text{m}$ band. However, a synthetic spectrum with the same set of values of $\log g$ and C/O as those used for the SWS6 and the KAO spectra, also fit our SWS1 observations well in the region $2.5\mu\text{m}$ to around $10\mu\text{m}$ if we adopt $T_{\text{eff}} = 3000$ K (instead of 3100 K). Fig. 5 shows the comparison between our observed ISO spectrum and a synthetic spectrum based on $(T_{\text{eff}}, \log g, C/O, K_p(C_3)) = (3000, -0.5, 1.023, {}^2K_p(C_3))$. The discrepancy long-ward of $10\mu\text{m}$ will be commented on in Sect. 7 below.

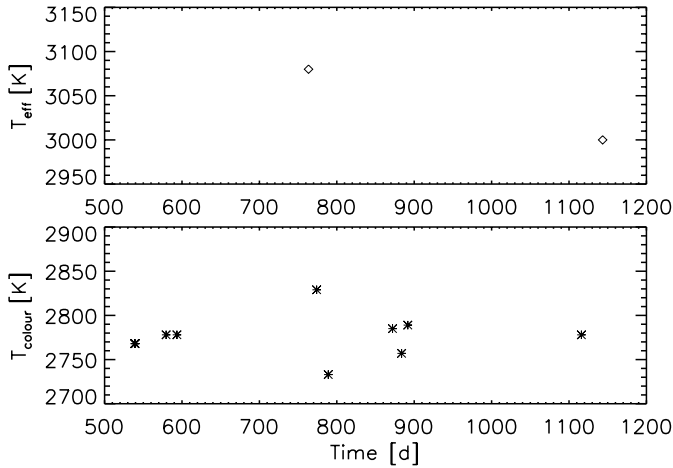


Fig. 6. Upper panel: The effective temperature of TX Psc, as derived from the analysis of 2 different infrared spectra, as function of date for the observation of the spectrum. Lower panel: Colour temperature derived by Baumert (1972) from Wing filter observations, as function of observational date of the photometry. There is a difference in the zero point of the dates in the two panels. The dates in the upper panel are Julian dates minus 2 449 650, while the lower panel is derived by subtracting JD 2 440 000.

As for the SWS6 and the KAO spectra our fit to the SWS1 spectrum is independent of the adoption of $K_p(C_3)$ for $(\log g, C/O) = (-0.5, 1.023)$, whereas a far too strong $5\mu\text{m}$ band is obtained if we choose $(\log g, C/O) = (0.0, 1.1)$ together with the ${}^1K_p(C_3)$ polynomial. In Fig. 4 we demonstrated the strong similarity of the spectra for $(\log g, C/O)$ equal to $(0.0, 1.1)$ and $(-0.5, 1.023)$ for models with $T_{\text{eff}} = 3100$ K. Also shown in Fig. 4 is the unrealistically strong $5\mu\text{m}$ feature resulting from the adoption of the ${}^1K_p(C_3)$ polynomial together with the parameter set $(\log g, C/O) = (0.0, 1.1)$.

4.4. The variation in T_{eff} between the time of our observation and other observations in the literature

AAVSO data show a total variation of a bit more than 1 magnitude in the estimated visual brightness of TX Psc. However, a part of this variation is due to a systematic difference between the estimates by different observers. If one looks at the values of a single observer, one typically sees an irregular light curve with an amplitude of around 0.5 magnitudes.

Tanaka et al. (1996) measured the variation in the infrared for a number of stars. They defined a colour index as the ratio of the flux at 6000 cm^{-1} and at 4500 cm^{-1} . By comparison with effective temperatures listed in Tsuji (1981) based on model atmospheres, they showed that this index is a good indicator of the effective temperature. The uncertainty in T_{eff} from the colour index is estimated to be 70 K (Tanaka et al. 1990). Two observations of TX Psc showed a difference in the estimated value of T_{eff} of somewhere between 100 K and 200 K depending on the assumed luminosity.

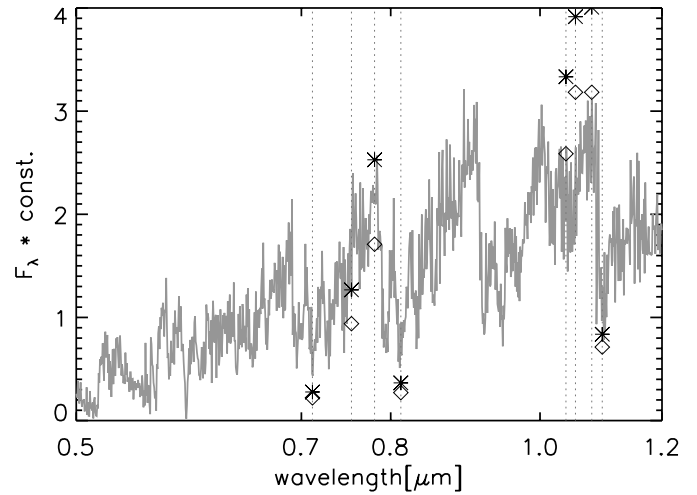


Fig. 7. Synthetic spectrum in the region $0.5\mu\text{m}$ to $1.2\mu\text{m}$ based on the same model as in Fig. 5, together with the observed Wing filter fluxes near minimum colour temperature (diamond symbols) and maximum colour temperature (star symbols).

Observations in the Wing filter system by Baumert (1972) at several times during two years, were transformed by him into a variation in colour temperature of approximately 100 K. The uncertainty in the colour temperature was estimated to be about 17 K. The $1.04\mu\text{m}$ magnitude in the Wing system corresponds approximately to the bolometric magnitude for TX Psc, and the observations in this filter showed a variation of 0.2 magnitudes. If the stellar radius is assumed constant, a bolometric flux variation of 0.2 mag also corresponds to a change in T_{eff} of approximately 100 K.

Fig. 6 (lower panel) shows the variation in the derived colour temperature by Baumert (1972), together with the two estimates of T_{eff} described above from the ISO spectra (upper panel). In general the value of the colour temperature is seen to be about 300 K lower than the effective temperature, but the size and time-scale of the variation of the colour temperature are in agreement with the corresponding numbers for T_{eff} derived from the spectra. The photometry therefore brings support to the idea that the overall difference between the spectrum by Aoki et al. (1998) (and the KAO spectrum) and ours is due to a temperature difference of approximately 100 K.

Since we estimate from the variation in Fig. 6 that our spectrum is taken near the minimum effective temperature of TX Psc, we compare in Fig. 7 our synthetic spectrum with the Wing filter fluxes near the minimum in colour temperature in Baumert's observations (diamond symbols in Fig. 7). It is seen that there is a good agreement between our model and the observed fluxes in this spectral region, too. For comparison also the observed filter fluxes for the maximum colour temperature in Baumert's observations (star symbols) are shown. We remark that the colour temperature in Fig. 6 seemingly can change substantially in a very short time.

We conclude from the above that all the existing infrared data of TX Psc in the $0.7\text{--}10\mu\text{m}$ region are consistent with a parameter set $(\log g, C/O) = (-0.5, 1.023)$ or $(0.0, 1.1)$ and

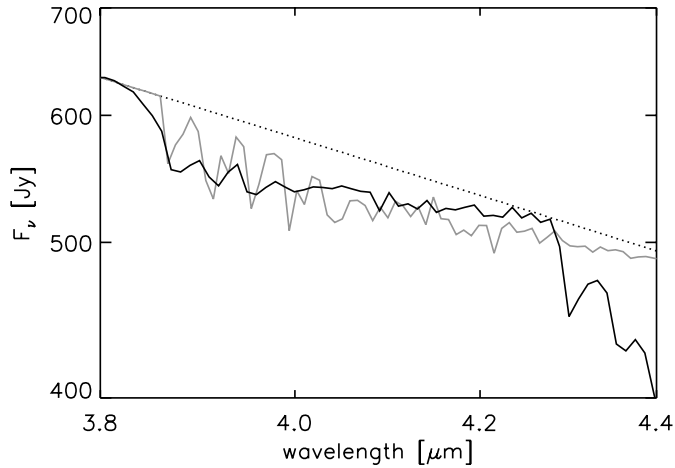


Fig. 8. Detail of the ISO spectrum (full line) and the synthetic spectrum (dotted gray line; computed as in Fig. 5) in the region around the CS first overtone system. The 3 to 4 first systems (between $3.8\mu\text{m}$ and $4\mu\text{m}$) are easily identifiable in the spectra. Long-ward of approximately $4.3\mu\text{m}$ the CO fundamental dominates the observed spectrum, whereas only the contribution from CS is included in the synthetic spectrum shown here. The black dotted almost straight line is the computed continuum.

T_{eff} varying by 100 K from 3100 K to 3000 K between the date of the ISO observations by Aoki et al. (1998) (and the KAO observations) and our ISO observations.

4.5. Contribution of individual molecules to the spectrum of TX Psc

In Fig. 11 we show the contribution of individual molecules and band systems to a synthetic spectrum of all the 3 stars discussed in this paper (see also Sect. 6.1). For TX Psc (middle panel) the spectra are based on a model with $(T_{\text{eff}}, \log g, C/O) = (3000, -0.5, 1.02)$. It is seen that there is a non-negligible contribution from C_2H_2 to the $3\mu\text{m}$ band for this model. For $T_{\text{eff}} = 3100\text{ K}$ the $3\mu\text{m}$ band of our synthetic spectrum of TX Psc is due almost solely to HCN, in agreement with the findings of Aoki et al. (1998). We notice further from Fig. 11 that the synthetic spectrum in the region short-ward of the $3\mu\text{m}$ feature is strongly suppressed relative to the model continuum. This depression is due to a combination of several bands of CO, CN, and C_2 . In the resolution of ISO, the observed continuum therefore is very different from the true continuum. In fact the model continuum and the ISO SWS1 continuum are only really close to one another at very few spectral regions. At most wavelengths the true continuum is not represented well by the observed continuum at this resolution.

The short wavelength side of the strong $5\mu\text{m}$ band is seen to be due to the fundamental band of CO, whereas the long wavelength side for many models is formed to a substantial part by C_3 . The C_3 contribution is strongest in models with high C/O. Our computed CO fundamental transition is weaker than in the observations (in contrast to the test computation of an oxygen-rich giant in Fig. 2 where the agreement between the computed and observed CO fundamental is very fine). However,

a small “discontinuity” in the observed shape of the $5\mu\text{m}$ band is visible in the observations of TX Psc (Fig. 5) at the wavelengths where we predict the start of the C_3 contribution to the band. This discontinuity is seen much more clearly in the spectra of V460 Cyg and TT Cyg than in the spectrum of TX Psc.

We confirm the identification of CS at $8\mu\text{m}$ (the fundamental vibrational transition) and at $4\mu\text{m}$ (the first overtone) by Aoki et al. (1998) as seen in Fig. 8. Also the weak contribution from CH around $4\mu\text{m}$ identified by Aoki et al. (1998) is confirmed in our spectra, although the individual CH and CS bands are not seen as clearly in our SWS1 spectrum as in their SWS6 spectrum, due to the difference in resolution.

Whereas the observed spectrum short-ward of $10\mu\text{m}$ is reproduced quite accurately by our model spectra (Fig. 5 and Fig. 7), it is also seen (Fig. 5) that the disagreement in the 12 to $20\mu\text{m}$ region is substantial, and of a qualitative character. This region (“the $14\mu\text{m}$ band”) will be discussed in detail in Sect. 7 for all the three observed stars together.

5. The spectrum of V460 Cyg

In the Rayleigh-Jeans approximation (i.e., $\lambda \rightarrow \infty$) to the Planck function, the slope (of the “continuum”) is independent of T_{eff} . Therefore we do not expect T_{eff} to manifest itself in the continuum flux at the SWS wavelengths (as it does for shorter wavelengths), and we also see from Fig. 1 that the continuum flux is basically identical for all the stars in the 3 to $10\mu\text{m}$ region of our spectra. The region long-ward of $10\mu\text{m}$ may, however, show a relative flux increase in V460 Cyg compared to TX Psc, which could be interpreted as a stronger dust contribution in V460 Cyg than in TX Psc, although the reduction of the observations in this region is more uncertain.

The main difference between the spectra of V460 Cyg and TX Psc (apart from the relative flux increase in V460 Cyg long-ward of $10\mu\text{m}$) is that the bands around $3\mu\text{m}$, $3.8\mu\text{m}$, and $7\mu\text{m}$ are weaker, while the long-wavelength part of the $5\mu\text{m}$ is stronger in the spectrum of V460 Cyg than in that of TX Psc. All the three former bands are dominated by the contribution of HCN, while the long-wavelength part of the $5\mu\text{m}$ band is due to C_3 .

The dissociation energies of HCN and C_3 are comparable and both molecules consist of 3 atoms. Therefore they have comparable temperature dependences. Since furthermore the amount of C_3 is roughly proportional to the amount of free (i.e., after the CO formation) carbon to the third power, while HCN needs only one carbon atom per molecule, the number ratio of C_3 to HCN is a strongly increasing function of C/O. We therefore interpret the spectral differences described above to be mainly due to a higher C/O ratio in V460 Cyg than in TX Psc. We also remark that the shape of the $5\mu\text{m}$ band in itself shows that the ratio between the contribution of C_3 and CO to this band is larger for V460 Cyg than for TX Psc, which we likewise interpret to mean that the C/O ratio is higher in V460 Cyg than in TX Psc.

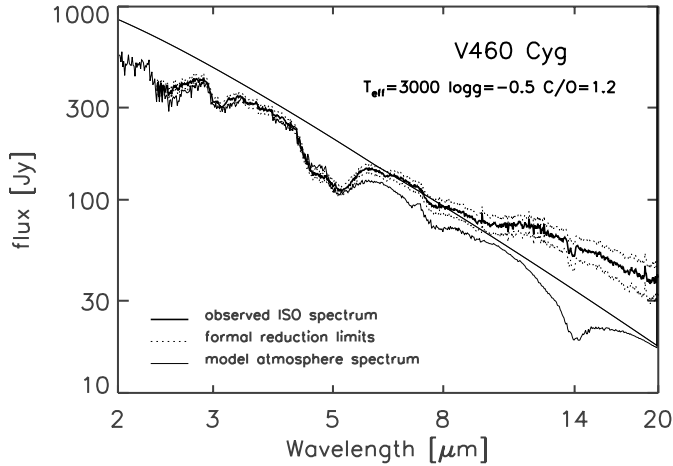


Fig. 9. The ISO SWS1 spectrum of V460 Cyg from $2.4\mu\text{m}$ to $20\mu\text{m}$ compared to a synthetic spectrum based on a model with $T_{\text{eff}} = 3000\text{ K}$, $\log g = -0.5$, and $C/O = 1.2$. Thick, thin, and dotted lines have the same meaning as in Fig. 5.

5.1. The fundamental parameters and the value of C/O

For V460 Cyg, values of T_{eff} spanning quite a wide range have been published in the literature (from 2850 K to 3200 K), as is seen in Table 1. The values at both ends of this interval are in contradiction with our ISO spectrum at the time of observation. The value $T_{\text{eff}} = 2850\text{ K}$ gives far too strong molecular bands almost throughout the observed spectrum, even for very low values of $\log g$. The value $T_{\text{eff}} = 3200\text{ K}$ on the other hand gives almost no $3\mu\text{m}$ band even for $\log g$ as high as 0.0. We therefore extended our grid of model atmospheres in particular around $T_{\text{eff}} = 2900\text{ K}$, 3000 K , and 3100 K for the analysis of this star. As for TX Psc, there is again no unique choice of fundamental parameters which gives the only possible fit to the $2\text{--}10\mu\text{m}$ region of our spectrum, but the values are better restricted because the C_3 feature at $5\mu\text{m}$ is more pronounced than in TX Psc, and the ratio between the $3\mu\text{m}$ and the $5\mu\text{m}$ intensity imposes important constraints on the possible combination of $\log g$ and C/O .

For $T_{\text{eff}} = 3000\text{ K}$ we obtain a good fit with $(\log g, C/O) = (-0.5, 1.2)$, provided ${}^2K_p(C_3)$ is used. For higher $\log g$, we were not able to find a reasonable fit by use of ${}^2K_p(C_3)$, whereas the adoption of the ${}^1K_p(C_3)$ polynomial (which favours formation of C_3) would imply a value of $\log g$ considerably smaller than -0.5 . We conclude that if $T_{\text{eff}} = 3000\text{ K}$, (1) a value of $K_p(C_3)$ close to ${}^2K_p(C_3)$ is most realistic, and (2) $(\log g, C/O) = (-0.5, 1.2)$ gives a good description of the whole spectral region, whereas (3) values of $\log g$ considerably larger than -0.5 cannot fit the $3\mu\text{m}$ band and the $5\mu\text{m}$ band simultaneously.

For $T_{\text{eff}} = 3100\text{ K}$ we can describe the spectrum between 2 and $10\mu\text{m}$ well with adoption of $(\log g, C/O) = (0.0, 1.2)$ and $K_p(C_3) = {}^2K_p(C_3)$. Increasing/decreasing $\log g$ will increase/decrease the intensity of both the $3\mu\text{m}$ and the $5\mu\text{m}$ bands, whereas increasing C/O will increase the ratio of the $5\mu\text{m}$ band to the $3\mu\text{m}$ band. For $K_p(C_3)$ close to the value of ${}^2K_p(C_3)$, $(\log g, C/O)$ is therefore confined relatively close to

$(0.0, 1.2)$. Since $\log g = 0.0$ is a bit above the HIPPARCOS values, $T_{\text{eff}} = 3100\text{ K}$ is an upper limit (if $K_p(C_3) = {}^2K_p(C_3)$). For $T_{\text{eff}} = 2900\text{ K}$, on the other hand, a lower value for $\log g$ of ≈ -1.5 is needed in order to reduce the general intensity of the bands. At those low values of T_{eff} and $\log g$ the chemical equilibrium is shifted in favour of a larger $5\mu\text{m}/3\mu\text{m}$ intensity ratio, which needs to be compensated by a lower C/O ratio, and we finally find a best fit for $T_{\text{eff}} \approx 2900\text{ K}$ by choosing $(\log g, C/O, K_p(C_3)) = (-1.5, 1.1, {}^2K_p(C_3))$. The listed $\log g$ values for V460 Cyg are likely to be underestimated in view of the very high luminosity resulting from the HIPPARCOS parallax. Therefore a $\log g$ of -1.5 is probably a bit too low, and we conclude that T_{eff} in the range 2950 K to 3050 K are the most acceptable values to fit the V460 Cyg ISO spectrum. If ${}^1K_p(C_3)$ is chosen instead of ${}^2K_p(C_3)$ the corresponding increased intensity of the $5\mu\text{m}$ band can be compensated for by choosing a lower C/O , but the resulting stronger $3\mu\text{m}$ band then has to be compensated for by choosing also a lower value for $\log g$. The value $(T_{\text{eff}}, \log g, C/O) = (3100, -0.5, 1.023)$ fits the spectrum well with $K_p(C_3) = {}^1K_p(C_3)$.

In summary, if $T_{\text{eff}} \approx 3000\text{ K}$, values of $(\log g, C/O) \approx (-0.5, 1.2)$ and $K_p(C_3)$ close to ${}^2K_p(C_3)$ fit the spectra well. If $T_{\text{eff}} \approx 3100\text{ K}$, $K_p(C_3)$ can be any of the two suggested values (because the computed $5\mu\text{m}$ band is weak for this high temperature), but $(\log g, C/O)$ have to be close to $(-0.5, 1.02)$ or close to $(0.0, 1.2)$ dependent on the choice of $K_p(C_3)$. For $T_{\text{eff}} \approx 2900\text{ K}$ $(\log g, C/O, K_p(C_3)) \approx (-1.5, 1.1, {}^2K_p(C_3))$ fits the spectrum well. In Fig. 9, we compare the observed spectrum to a synthetic spectrum based on a model with $T_{\text{eff}} = 3000\text{ K}$, $\log g = -0.5$, $C/O = 1.2$, and ${}^2K_p(C_3)$.

6. The spectrum of TT Cyg

The spectrum of TT Cyg follows the same trend as we saw from TX Psc to V460 Cyg, with a stronger $5\mu\text{m}$ feature in the region where C_3 tends to dominate the band. We interpret this to mean that the C/O ratio must be larger in TT Cyg than in any of the two other stars, and we can simulate the ratio of the $5\mu\text{m}$ and the $3\mu\text{m}$ intensities well with $C/O \approx 1.5$ (if $K_p(C_3) \approx {}^2K_p(C_3)$). On the other hand, the absolute intensity of the $3\mu\text{m}$ band is in-between that of TX Psc (on the date of our observations) and that of V460 Cyg. Since an increase in C/O alone would tend to weaken the $3\mu\text{m}$ feature, T_{eff} of TT Cyg therefore has to be lower than that of V460 Cyg and/or the gravity must be higher (both effects would cause stronger polyatomic bands in general). T_{eff} can be as high as that of TX Psc (or even slightly higher if $\log g$ is in the very high end of what is predicted by the HIPPARCOS data), because the weaker $3\mu\text{m}$ feature in TT Cyg than in TX Psc then can be due to the higher C/O in TT Cyg than in TX Psc.

We obtain a good agreement between the observed and the computed spectrum for the parameter set $(T_{\text{eff}}, \log g, C/O, K_p(C_3)) = (3000, 0.0, 1.5, {}^2K_p(C_3))$. If T_{eff} is lower than this the polyatomic bands will be stronger, which can be compensated by also lowering the gravity in the model, and therefore also the parameter set $(T_{\text{eff}}, \log g, C/O, K_p(C_3)) = (2900, -1.0,$

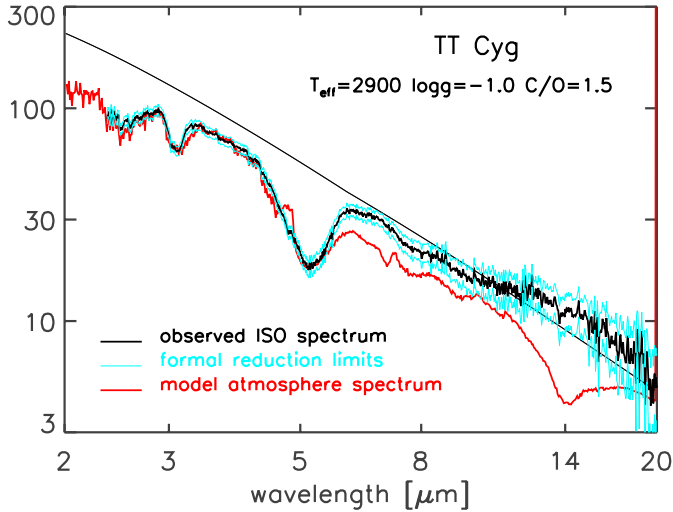


Fig. 10. The ISO SWS1 spectrum of TT Cyg from $2.4\mu\text{m}$ to $20\mu\text{m}$ compared to a synthetic spectrum based on a model with $T_{\text{eff}} = 2900$, $\log g = -1.0$, and $\text{C/O} = 1.5$. Thick, thin, and dotted lines have the same meaning as in Fig. 5.

$1.5, {}^2\text{K}_p(\text{C}_3)$ gives good agreement with the observed spectrum. Fig. 10 compares a synthetic spectrum based on a model with $(T_{\text{eff}}, \log g, \text{C/O}, \text{K}_p(\text{C}_3)) = (2900, -1.0, 1.5, {}^2\text{K}_p(\text{C}_3))$ with our ISO data. Since $\log g = -1.0$ is a bit below the value inferred from the HIPPARCOS data, we conclude that also $T_{\text{eff}} = 2900$ K is a lower limit. Increasing T_{eff} to a value considerably larger than 3000 K, on the other hand, would demand an unusual large value of $\log g$. We therefore conclude that T_{eff} in the range 2950 K to 3050 K are the most acceptable values also for TT Cyg. Substituting ${}^2\text{K}_p(\text{C}_3)$ with ${}^1\text{K}_p(\text{C}_3)$ gives larger weight to the formation of C_3 , which has to be compensated with a lower C/O ratio in order to still fit the observed spectrum. Our synthetic spectra based on models with $(T_{\text{eff}}, \log g, \text{C/O}, \text{K}_p(\text{C}_3)) = (3000, 0.0, 1.2, {}^1\text{K}_p(\text{C}_3))$ and (to some extent) $(T_{\text{eff}}, \log g, \text{C/O}, \text{K}_p(\text{C}_3)) = (2900, -1.0, 1.3, {}^1\text{K}_p(\text{C}_3))$ therefore also result in good agreement with our ISO spectrum of TT Cyg.

6.1. Molecules contributing to the synthetic spectra

Fig. 11 shows the most important of the molecules contributing to the synthetic spectra for three models representing the observed stars. The individual spectra are normalised to the local continuum and shifted relative to one another in order to increase the clarity of the figure. From top to bottom the three panels in Fig. 11 represent V460 Cyg, TX Psc, and TT Cyg. The individual spectra in each panel are based on the same model atmosphere structure.

Comparing the three panels we notice that (1) the intensity of the CS bands is quite similar in all three stars, but in particular the first overtone is slightly stronger in the model of TX Psc than in the two other models. (2) The intensity of the HCN bands increases in the sequence V460 Cyg, TT Cyg, TX Psc. Containing only one carbon atom, HCN is relatively strong for

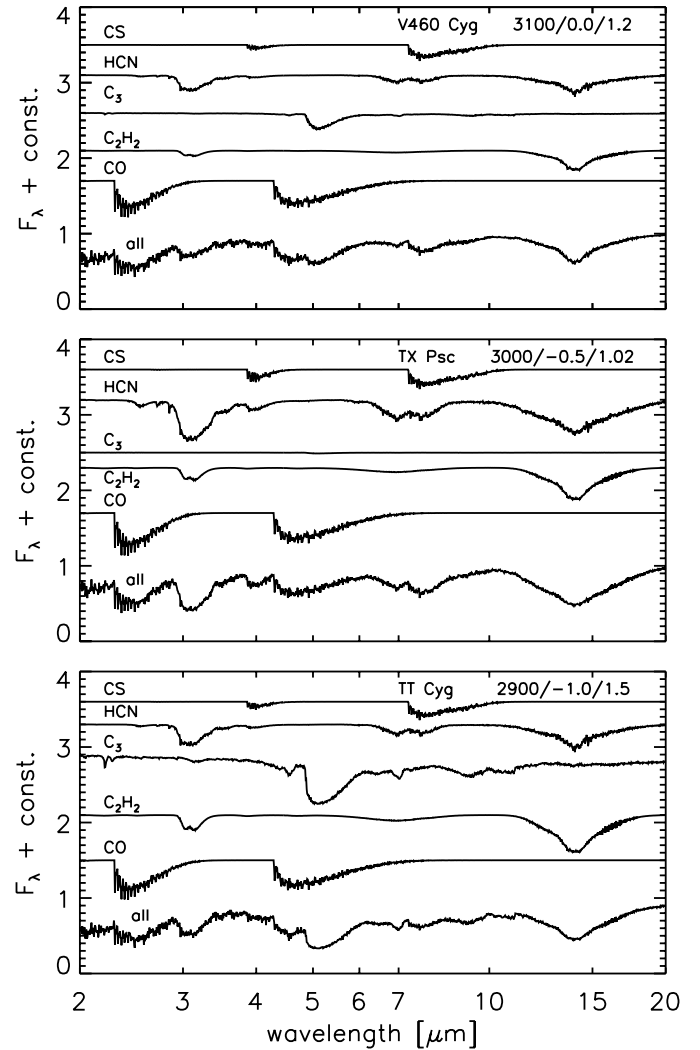


Fig. 11. The individual contributions of CS, HCN, C_3 , C_2H_2 , and CO to synthetic spectra representing the three stars analysed in the present paper. The three models represent a sequence of decreasing effective temperature (3100 K, 3000 K, and 2900 K), decreasing $\log g$ (0.0, -0.5 , and -1.0), and C/O ratios 1.2, 1.023, 1.5. Also shown is the full synthetic spectrum. All spectra in this figure are normalised to the corresponding continuum.

low C/O ratios, but also T_{eff} and $\log g$ play a role. (3) Having 3 carbon atoms, C_3 is very sensitive to C/O, and the opacity of C_3 in TT Cyg is therefore much stronger than in the two other stars. (4) Although the opacity of C_2H_2 is an increasing function of $\log g$ it is seen that decreasing T_{eff} is more important. The contribution of C_2H_2 to the spectral features is therefore increasing for the sequence V460 Cyg, TX Psc, TT Cyg. (5) As for CS, the intensity of the CO bands is quite comparable in the three stars. (6) Among the remaining molecules, in particular the contribution of C_2 differs between the three stars, and it is the resulting stronger absorption in the $2.5\mu\text{m}$ region for high C/O ratios that is responsible for the better fit to this region for V460 Cyg and TT Cyg than for TX Psc.

A more detailed description of the contribution of molecules to the spectra in our models of carbon stars, has recently been published by Loidl et al. (1999).

7. The 14 μm region and beyond in the spectra of V460 Cyg, TT Cyg, and TX Psc

As can be seen from several of the previous figures, the quality of the fit to the spectral region long-ward of approximately 10 μm is much poorer than the quality of the fit short-ward of this wavelength. The reason for this discrepancy is not clear, and it may well hold some of the most interesting informations about the cool carbon stars in the ISO project, not yet understood. Unfortunately, the reduction of the data is also most uncertain in this region, as discussed in Sect. 2. In the following we will assume that the reduction is correct, with a small risk that it may later turn out that part of the discrepancy we try to explain is due to a poorly calibrated response-function of the SWS detector in the long-wavelength spectral range for low count rates.

There are two major discrepancies between the synthetic and the observed spectrum in the long wavelength region. *First*, the slope differs considerably. If this has a physical reason, it could be explained by a contribution from a continuous dust emission. *Second*, we predict a strong photospheric “14 μm ” band, while the observed spectra show almost a feature-less, continuum-like structure throughout this spectral interval.

7.1. The spectral slope in the long-wavelength region

In order to throw more light on the question about the physical reality of the discrepancy between the observations and our computed spectra in the long-wavelength region, we extracted several SWS1 spectra of oxygen-rich late type stars from the ISO archive. Oxygen-rich stars are not expected to have a “14 μm ” feature. We therefore reduced the ISO spectra of the oxygen-rich stars in the same way as we did for our 3 carbon-rich stars. Fig. 2, which was discussed in detail in Sect. 2, compares the ISO archive spectrum of HR 6705 with our computed synthetic spectrum of an oxygen-rich giant with $T_{\text{eff}} = 3850$, $\log g = 0.0$, and $Z = Z_{\odot}$ (including $\text{C/O} = 0.43$; the solar value). This spectrum has approximately the same detector count-rate in the 10–20 μm region as our spectra of TX Psc and V460 Cyg. It is seen that the observed and the synthetic spectra of HR 6705 are in good mutual agreement within the observational uncertainty. We therefore conclude that the discrepancy between the observed and the computed spectral slope of our 3 carbon-rich stars are unlikely to be an effect of the way the spectra are reduced or due to problems in the spectral response function of the ISO instruments.

The continuum sources included in our computation of oxygen-rich and carbon-rich spectra are the same (dominated by H^- in this spectral region) and quite insensitive to the C/O ratio. Our computed continuum slopes are also comparable for the two types of stars. We therefore conclude that the discrepancy between the slopes of the computed and observed spectra

of the carbon-rich stars is unlikely to be due to the computed photospheric continuum. It is not likely to be caused by lacking strong molecular absorption in the carbon star models either, because the observed spectra tend to be above the computed continuum (at least for V460 Cyg and TT Cyg; see Fig. 9 and Fig. 10). We are therefore left with the conclusion that the discrepancy between the observed and computed slopes of the carbon star spectra most likely have their origin in a real physical phenomenon which is not present in general in corresponding oxygen-rich stars.

We remark that the general agreement between the computed and observed spectra immediately short-ward of 10 μm , say the 6–10 μm region, is poorer for V460 Cyg and TT Cyg than it is for TX Psc, although the intensity and form of individual bands, as for example the 8 μm CS feature, are in good agreement for all 3 stars. TX Psc is “almost an S-star”, with C/O lower than that of the two other stars. The difference between the fits for the 3 stars in this region could therefore in principle be due to the C_3 absorption coefficient (which is pseudo-continuous and relatively uncertain in this spectral range) or it could be due to dust emission (discussed below) which could be more efficient for higher values of C/O .

7.2. The absorption in the 14 μm region

The second type of discrepancy mentioned above (the 14 μm feature), is of a qualitatively different character. Compared to the computed spectrum, the observed “14 μm ” band is quite weak, and it consist of, or includes, a narrow, well defined absorption just short-ward of 14 μm . In contrast, our computed 14 μm band is broad and strong. If the 14 μm band forms at the photospheric depths and temperatures which self-consistent model atmosphere computations predict, it has to be very broad, because many hot-band transitions contribute to the observed band. The anharmonicity constants determining the broadness of such an absorption feature in a hot gas, are very well determined from laboratory experiments. Therefore we can be relatively certain that we do not see a pure photospheric spectrum in the long-wavelength region of the ISO spectra.

However, we do not see a so-called warm molecular envelope either, which has been introduced in the literature and discussed by several authors in order to explain discrepancies between computed molecular bands and the observed spectra (e.g., Tsuji et al. 1997; Yamamura et al. 1998; 1999). The idea of the warm molecular envelope is to introduce one or more detached, relatively dense layers of molecular gas above the photosphere. Temperatures and densities are free parameters (i.e. values not predicted by the self-consistent computations of the photosphere, and not by a hydrodynamical wind either) which can be adjusted in order to increase (i.e., absorption) or decrease (i.e., emission) the computed photospheric band intensities until they fit the observed intensities.

An important evidence that the 14 μm region cannot be explained by introduction of a warm molecular envelope is seen in the fine fit of, in particular, the 3 μm band based on photospheric models alone. The 3 μm band and the 14 μm band will

respond parallel to changes in the temperature structure. The intrinsic transition probabilities that give rise to the two bands are very similar, and the separation in the excitation energies of the vibrational levels that give rise to the hot-bands are almost identical in the two cases. This means that any temperature inversion in (or dense molecular layer above) the photosphere that could weaken the $14\ \mu\text{m}$ band would create a similar weakening of the $3\ \mu\text{m}$ band. However, the $3\ \mu\text{m}$ band is well reproduced in all our photospheric synthetic spectra as is seen in Fig. 5, 9, and 10.

We therefore conclude that we do not see a simple photospheric (with or without addition of a postulated warm molecular layer contribution) $14\ \mu\text{m}$ band in the observed carbon star spectra.

7.3. Discussion of the long-wavelength discrepancy

Three natural questions therefore arise: (1) Why do we not see the photospheric $14\ \mu\text{m}$ band when we do see the corresponding photospheric $3\ \mu\text{m}$ band? (2) what is the narrow and weak feature we see just short-ward of $14\ \mu\text{m}$ in all three spectra? and (3) which relation (if any) does the lack of a photospheric $14\ \mu\text{m}$ feature have to the discrepancy between the observed and computed slope in the $10\text{--}20\ \mu\text{m}$ region?

Yamamura et al. (1998) analysed the shape of the feature just short-ward of $14\ \mu\text{m}$ in the ISO SWS spectra of 11 carbon stars. The authors normalised the continuum to the local observed continuum level, which in the relatively narrow spectral region they analysed ($13\ \mu\text{m}$ to $15\ \mu\text{m}$) left basically only the small feature at $13.7\ \mu\text{m}$. They then compared the shape of this feature with laboratory data for room temperature line lists of C_2H_2 . The synthetic spectra used in the analysis were based on two layers of homogeneous, detached molecular gas, in which the two temperatures and densities were adjusted until a good fit to the spectrum was obtained. A similar approach was used to explain bands of SO_2 , H_2O , and SiO in ISO spectra of M giants (Yamamura et al. 1999). While this can be a useful approach for classifying the observed features, it of course gives no insight into the physical character of the absorption process (among other things because of the lack of self-consistency in this very simplified model and spectrum computation).

Several questions were therefore left unsolved in Yamamura et al.'s work, such as: How are the proposed two layers of C_2H_2 gas formed? Why are the $14\ \mu\text{m}$ and the $3\ \mu\text{m}$ bands mutually inconsistent? Can low-resolution stellar spectra really be analysed based on laboratory, room-temperature line lists? Can one safely just ignore the difference in the continuum slope between the computed and the observed spectra?

In order to approach the question of what we actually see in the ISO spectra in the $14\ \mu\text{m}$ region, we will for a short moment ignore (1) the inconsistency with the $3\ \mu\text{m}$ region spectrum, (2) the question of how the photospheric spectrum disappeared, and (3) the question of the spectral slope, and first analyse the appearance of a C_2H_2 spectrum alone, under various relevant conditions, and then return to the general questions in the next section.

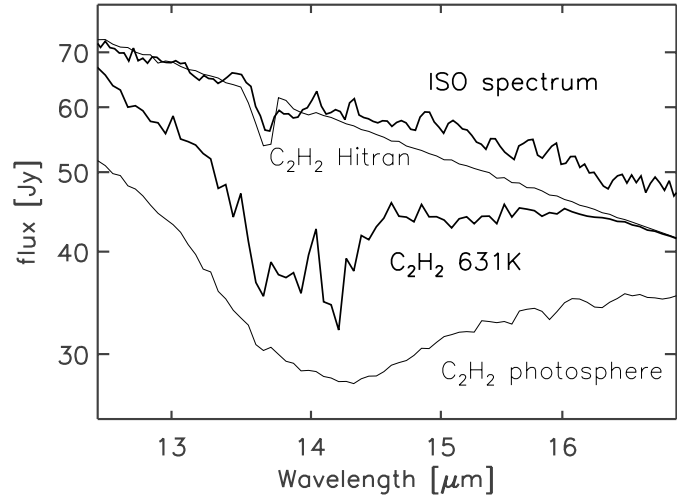


Fig. 12. Our ISO SWS1 spectrum of TX Psc in the $14\ \mu\text{m}$ region compared to synthetic spectra based on a model atmosphere with $T_{\text{eff}} = 3000\ \text{K}$, $\log g = 0$, and $\text{C}/\text{O} = 1.1$. From top to bottom the spectra are: (1) thick line: the observed spectrum, (2) thin line: computed spectrum of C_2H_2 based on the HITRAN line list, (3) thick line: computed C_2H_2 spectrum based on an OS at fix temperature 631 K, and (4) thin line: full C_2H_2 spectrum from complete line list (OS) at the correct photospheric temperatures.

In Fig. 12 we compare the observed ISO spectrum of TX Psc in the $14\ \mu\text{m}$ region with a number of spectra of C_2H_2 (only), all based on a model atmosphere of TX Psc which fits the spectrum well in the region short-ward of $10\ \mu\text{m}$ (as seen in Fig. 5). The upper most thick line spectrum (1) is the observed spectrum. The thin line spectrum just below it (2) denotes a spectrum based only on the C_2H_2 lines from the HITRAN data base (Rothman et al. 1992). It is seen that there is a remarkable agreement between the computed and the observed spectral feature at $13.7\ \mu\text{m}$ (in particular if we normalised the computed spectrum to the local continuum, as is done for example in the work of Yamamura et al. 1998). This is quite surprising and unexpected, because this computed spectrum is inconsistent with the computed model atmosphere, and the contributions of HCN and C_3 are excluded. The line list in the HITRAN data base is, like most other laboratory line lists, measured at room temperature. For most molecules (including C_2H_2) the electronic and vibrational ground level strongly dominates the population at room temperature, and the rotational levels are populated only up to modest values of the J quantum number, compared to those values that play a role at stellar temperatures. This is the reason for the sharp and narrow absorption centred at $13.7\ \mu\text{m}$. Only lines with J quantum number up to 35 are included, and only from low vibrational levels. These lines will only contribute a tiny fraction of the C_2H_2 opacity at stellar atmospheric temperatures.

The thick line spectrum (3) in the middle of Fig. 12 is a C_2H_2 spectrum computed based on the OS absorption coefficient at 631 K only (i.e., the C_2H_2 opacity at all model layers is computed based on the correct C_2H_2 partial pressures but the 631 K absorption coefficient). This spectrum is also incon-

sistent with the computed model atmosphere, but it illustrates approximately how the C_2H_2 spectrum would appear in a gas of a temperature around this value. Finally, the lowest thin line spectrum (4) in the figure shows the full C_2H_2 photospheric spectrum. This is the only one of the three synthetic spectra in Fig. 12 which is self-consistent with the model atmosphere computation. I.e., this is how the C_2H_2 contribution to the spectrum would appear if we see a pure photospheric spectrum, just as we do in the short-wavelength part of the ISO spectra. We do recognise the $13.7 \mu m$ feature also in these two lower spectra of Fig. 12, although they are successively less pronounced. We also notice that we do recognise in the ISO spectrum a feature from approximately $14.0 \mu m$ to $14.3 \mu m$ which is very strong in the 631 K synthetic spectrum, and maybe also some of the other small wiggles. We therefore conclude that it seems as if the ISO spectra of the three carbon stars in the $14 \mu m$ region show a gas of very low temperature (cooler than 600 K) and very rich in C_2H_2 . We also notice that there are indications in the detailed comparisons between the synthetic spectra at various temperatures that we can follow the C_2H_2 part of the “ $14 \mu m$ feature” considerably beyond $14 \mu m$ as expected from a gas of higher-than-room temperature.

7.4. A tentative model to explain the full SWS spectral region

In conclusion from the above discussion one could envision the discrepancy between the observed and computed long-wavelength spectral slope to be due to a dust emission, while the $14 \mu m$ region absorption spectrum could be interpreted as being dominated by absorption in a C_2H_2 -rich gas with a temperature above 300 K but below ≈ 600 K.

In order to explore this scenario, we simulated combined dust and gas spectra, firstly by adding a Planck function emission of low temperature to our photospheric spectrum and secondly by using our photospheric dust-free spectra as input for the dust-envelope spectrum computation program DUSTY (Ivezić & Elitzur 1995). DUSTY solves the radiative transfer problem for a source embedded in a spherically symmetric dusty envelope. The spectrum of the central source, the dust condensation temperature, grain properties, radial density distribution and total optical depth are specified in advance. The idea of both of these exercises is of course to see if the whole observed spectrum can be explained qualitatively by a relatively hot photospheric component which dominates the flux in the near infrared (say below $10 \mu m$) and a relatively cool emission (dust) component above the photosphere, which obscures the long-wavelength photospheric spectrum. This is in contrast to work presented by Aoki et al. (1999) and Yamamura et al. (1998) who attempted to fit only the long-wavelength part of the ISO spectrum, ignoring the consequences on the fit of the short-wavelength ISO spectrum (Aoki et al. 1998).

Representative results of our tests for TX Psc are shown in Fig. 13. For the DUSTY calculations we used a photospheric spectrum with the parameters $(T_{\text{eff}}, \log g, C/O, K_p(C_3)) = (3000, -0.5, 1.023, {}^2K_p(C_3))$. We adopted pure carbon dust and the DUSTY standard grain size distribution. For both types of simu-

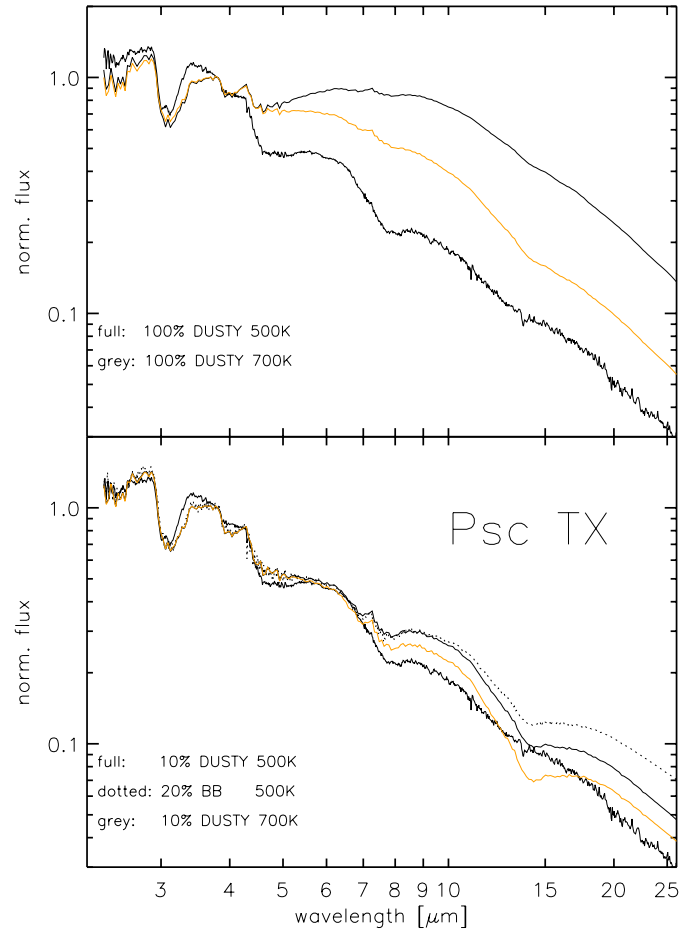


Fig. 13. Comparison of our ISO spectrum of TX Psc (thick line) with model spectra including emission from dust. The upper panel gives the spectra with full dust-envelopes (100% contribution) having condensation temperatures of 500 K and 700 K, a r^{-4} density law and an optical depth at $2 \mu m$ of 0.05. The lower panel shows the same dust-envelopes but now assuming only a 10% contribution and it shows also the effect of a 20% contribution from a 500 K blackbody. See Sect. 7.4 for details.

lations it was clear after a few tests that a (dust) emission component covering the whole stellar surface had to be excluded (upper panel of Fig. 13). In both approaches we found it impossible to fill in the photospheric $14 \mu m$ band (such that even a qualitative agreement with the observations in this region could be obtained) without also destroying the fine agreement between the observed and computed photospheric short-wavelength part of the SWS spectral region. We therefore experimented with various choices of a filling factor, i.e. only a certain fraction of the (dust) emission is added to the photospheric spectrum. It was also clear that only a steep density fall-off ($1/r^4$) and small optical depths could produce reasonable fits. The best results were found for dust condensation or blackbody temperatures of ≈ 500 K and filling factors between 0.1 and 0.2.

We see these results as pointing at a rather complex structure in the upper atmospheric region of carbon stars. Summarising, the slope of the long-wavelength region and the “filling in” of the $14 \mu m$ band but not the $3 \mu m$ (and the $5 \mu m$) band(s) can

be partly understood by the influence of a continuous emission source on top of the photosphere. The simulations indicate however, that this source cannot cover the entire surface. We therefore tentatively suggest that the photosphere is obscured by clumps of dust-rich cool gas which cover about 10% (the filling factor) of the surface area. The features seen at $13.7\ \mu\text{m}$, $14.0 - 14.3\ \mu\text{m}$, and possible other small discrete absorptions in the region, are due to C_2H_2 (and possible HCN) absorption in the very cool gas above the region of these clumps. However, we stress that this scenario is not a self-consistent, physical model computation, but a suggestion.

Another possible explanation, which will be explored together with this possible scenario in the near future, are dynamical effects in the outer atmosphere. Detailed and self-consistent hydrodynamic models and corresponding synthetic spectra in spherical geometry might lead to a better agreement with the ISO spectra. Such an approach was tested by us for the carbon star R Scl (Hron et al. 1998) without a clear and definitive answer, but was successfully for cool M-giants in explaining trends in the SiO equivalent widths (Aringer et al. 1999) which had previously been attributed to effects of a hypothetical warm molecular envelope (Tsuji et al. 1997).

Recent lunar occultation observations (Richichi et al. 1995) and IR imaging (Cruzalèbes et al. 1998) support the idea of an inhomogeneous atmosphere of cool carbon stars (although at much larger distances from the star than modelled in the present paper). Also IUE and HST observations of carbon stars in the ultraviolet (Eriksson et al. 1986; Johnson et al. 1988; Johnson et al. 1995) points at the necessity of the introduction of considerable inhomogeneities in the atmospheric structure, and a filling factor for the hot chromospheric material was estimated to be around 10% (Jørgensen & Johnson 1991) in order to explain both the UV spectrum and the strongest photospheric CO lines. If all these observational and theoretical interpretations are correct, a very complex picture of the upper atmospheric region of cool carbon giants is emerging.

8. Conclusions

We have obtained ISO SWS1 spectra of the three carbon stars TX Psc, V460 Cyg, and TT Cyg, in the full range from $2.4\ \mu\text{m}$ to $20\ \mu\text{m}$ (and beyond). We have analysed the spectra by use of self-consistent, hydrostatic, MARCS model atmospheres, and high-resolution opacity sampling synthetic spectra. Among the results we have presented we note that:

- The ISO SWS spectra impose important new constraints on the values of the fundamental parameters of giant carbon stars. Among the parameters is the value of $\log g$ which is difficult to estimate from spectral features in other spectral regions.
- Comparison of our ISO spectrum of TX Psc with another ISO spectrum published in the literature (Aoki et al. 1998) and with an older Kuiper Airborne Observatory spectrum (Goebel & Johnson 1984), shows that the star has changed effective temperature with $\Delta T_{\text{eff}} \approx 100\ \text{K}$ between the three

observations. The debate in the literature about the exact value of C/O for TX Psc cannot be resolved by the ISO observations alone as long as an unusual large uncertainty in the physical parameter $K_p(\text{C}_3)$ persists.

- Our ISO spectra can be best fitted with models of T_{eff} close to 3000 K for all three stars, and values of the gravity decreasing an order of magnitude from TX Psc and TT Cyg to V460 Cyg. A pronounced effect on the spectra is due to an increasing sequence of C/O from close to 1 for TX Psc over $\text{C/O} \lesssim 1.2$ for V460 Cyg to $\text{C/O} \lesssim 1.5$ for TT Cyg.
- The ratio of the intensity of the $3\ \mu\text{m}$ feature (due to C_2H_2 and HCN) to the intensity of the $5\ \mu\text{m}$ feature (due to CO and C_3) is a sensitive measure of the C/O ratio.
- While the strong $3\ \mu\text{m}$ and $5\ \mu\text{m}$ bands can be modelled accurately by a dust-free, plane parallel, hydrostatic photosphere, the “ $14\ \mu\text{m}$ region” is not consistent with a photospheric spectrum.
- Previous studies have pointed at inhomogeneities in images of cool carbon stars, and models have suggested clumps of hot chromospheric gas moving through the outer atmosphere. The observed excess flux compared to synthetic spectra long-ward of $\approx 10\ \mu\text{m}$, and the filling of the $14\ \mu\text{m}$ band can not be modelled with a simple one component photosphere. We propose that clumps of cool material of $\approx 500\ \text{K}$ form in the upper part of the atmosphere and obscure about 10% of the surface area, and that the weak features seen around $13.7\ \mu\text{m}$ originate in cooler layers above the region of these clumps. Dynamical effects in the upper atmosphere might be also important. Hence in summary, the ISO spectral region seems to include a much more complex and challenging region of the carbon star atmospheres than we have previously been able to study from visual spectra.

Acknowledgements. Discussions with T.Tsuji and Ch.Helling concerning the $K_p(\text{C}_3)$ polynomial are greatly acknowledged. This work was supported by the Austrian Science Fund (FWF project S7308-AST), the Austrian Academy of Sciences (RL acknowledges a ‘Doktorandenstipendium’), and the Danish Natural Science Research Council. The ISO Spectral Analysis Package (ISAP) is a joint development by the LWS and SWS Instrument Teams and Data Centers. Contributing institutes are CESR, IAS, IPAC, MPE, RAL and SRON.

References

- Aoki W., Tsuji T., Ohnaka K., 1998, A&A 340, 222
- Aoki W., Tsuji T., Ohnaka K., 1999, A&A 350, 945
- Aringer B., Höfner S., Wiedemann G., et al., 1999, A&A 342, 799
- Baumert J.H., 1972, Ph.D. Thesis, The Ohio State University
- Chandra S., Kegel W.H., Le Roy R.J., Hertenstein T., 1995, A&AS 114, 175
- Cruzalèbes P., Lopez B., Bester M., Gendrun E., Sama B., 1998, A&A 338, 132
- de Graauw T., Haser L.N., Beintema D.A., et al., 1996, A&A 315, L49
- De Laverny P., Gustafsson B., 1998, A&A 332, 661
- Dyck H.M., Van Belle G.T., 1996, AJ 112, 1, 294
- Eriksson K., Gustafsson B., Johnson H.R., et al., 1986, A&A 161, 305
- Goebel J.H., Johnson H.R., 1984, ApJ 284, L39
- Goorvitch D., 1990, ApJS 74, 769

- Goorvitch D., Chackerian C. Jr., 1994, *ApJS* 91, 483
- Gustafsson B., Bell R.A., Eriksson K., Nordlund Å., 1975, *A&A* 42, 407
- Helling C., Jørgensen U.G., Plez B., Johnson H.R., 1996, *A&A* 315, 194
- Hron J., Loidl R., Höfner S., et al., 1998, *A&A* 335, L69
- Höfner S., Dorfi E.A., 1997, *A&A* 319, 648
- Höfner S., Jørgensen U.G., Loidl R., Aringer B., 1998, *A&A* 340, 497
- Ivezić Ž., Elitzur M., 1995, *ApJ* 445, 415
- Johnson H.R., Eaton J.A., Querci F., Querci M., Baumert J.H., 1988, *A&A* 204, 147
- Johnson H.R., Ensmann L., Alexander D.R., et al., 1995, *ApJ* 443, 281
- Jørgensen U.G., 1989, *ApJ* 344, 901
- Jørgensen U.G., 1990, *A&A* 232, 420
- Jørgensen U.G., 1997, In: van Dishoeck E.F., *Molecules in Astrophysics: Probes and Processes*. Kluwer, p. 441
- Jørgensen U.G., Johnson H.R., 1991, *A&A* 244, 462
- Jørgensen U.G., Larsson M., 1990, *A&A* 238, 424
- Jørgensen U.G., Almlöf J., Gustafsson B., Larsson M., Siegbahn P., 1985, *J. Chem. Phys.* 83, 3034
- Jørgensen U.G., Almlöf J., Siegbahn P.E.M., 1989, *ApJ* 343, 554
- Jørgensen U.G., Johnson H.R., Nordlund Å., 1992, *A&A* 261, 263
- Jørgensen U.G., Larsson M., Iwamae A., Yu B., 1996, *A&A* 315, 204
- Kurucz R.L., 1994, In: Jørgensen U.G. (ed.) *Molecules in the Stellar Environment*. Lecture Notes in Physics vol. 428, Springer-Verlag, p. 282
- Lambert D.L., Gustafsson B., Eriksson K., Hinkle K.H., 1986, *ApJS* 62, 373
- Leech K., 1998, *SWS Instrument Data Users Manual Issue 1.0*, SAI/98-195/Dc, ESA
- Loidl R., Höfner S., Jørgensen U.G., Aringer B., 1999, *A&A* 342, 531
- Ohnaka K., Tsuji T., 1996, *A&A* 310, 9330
- Querci F., Querci M., Tsuji T., 1974, *A&A* 31, 265
- Quirrenbach A., Mozurkewich D., Hummel C.A., Buscher D.F., Armstrong J.T., 1994, *A&A* 285, 541
- Richichi A., Chandrasekhar T., Lisi E., et al., 1995, *A&A* 301, 439
- Ridgway S.T., Joyce R.R., White N.M., Wing R.F., 1980, *ApJ* 235, 126
- Rothman L.S., Gamache R.R., Tipping R.H., et al., 1992, *JQSRT* 48, 469
- Sørensen G.O., Jørgensen U.G., 1992, *J. Chem. Phys.* 97, 4616
- Tanaka W., Hashimoto O., Nakada Y., et al., 1990, *NAOJ* 1, 3, 259
- Tanaka W., Okada T., Hashimoto O., Yamamura I., Tanabé T., 1996, *NAOJ* 4, 3, 135
- Tsuji T., 1973, *A&A* 23, 411
- Tsuji T., 1981, *JA&A* 2, 95
- Tsuji T., Ohnaka K., Aoki W., 1997, *A&A* 320, L1
- Walker A.R., Wild P.A.T., Byrne P.B., 1979, *MNRAS* 189, 455
- Yamamura I., de Jong T., Justtanont K., Cami J., Waters L.B.F.M., 1998, *Ap&SS* 255, 351
- Yamamura I., de Jong T., Onaka T., Cami J., Waters L.B.F.M., 1999, *A&A* 341, L9